Supplementary Information

Ion-modulated structure, proton transfer, and capacitance in the Pt(111)-water electric double layer

Xiaoyu Wang,[1] Junmin Chen,[1] Zezhu Zeng,[2] Frederick Stein,[3] Junho Lim,[4,1] and Bingqing Cheng[1,2,5,6,7,*]

[1] *Department of Chemistry, UC Berkeley, California 94720, United States*

[2] *The Institute of Science and Technology Austria, Am Campus 1, 3400 Klosterneuburg, Austria*

[3] *Center for Advanced Systems Understanding (CASUS), Helmholtz Zentrum Dresden-Rossendorf, Germany*

[4] *Department of Chemistry, Pohang University of Science and Technology (POSTECH), South Korea*

[5] *Materials Sciences Division, Lawrence Berkeley National Laboratory, Berkeley, CA, USA*

[6] *Chemical Sciences Division, Lawrence Berkeley National Laboratory, Berkeley, CA, USA*

[7] *Bakar Institute of Digital Materials for the Planet, UC Berkeley, California 94720, United States*

(Dated: April 17, 2026)

* bingqingcheng@berkeley.edu

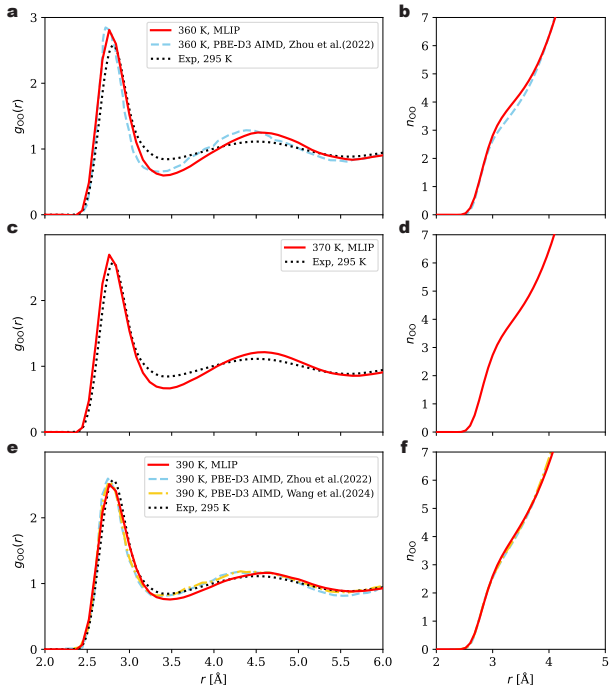

Figure S1. Oxygen-oxygen radial distribution functions ($g_{OO}(r)$) and running coordination numbers ($n_{OO}(r)$) of bulk liquid water at (a,b) 360 K, (c,d) 370 K, and (e,f) 390 K with a fixed density of 0.997 g/ml. The results are compared with previous AIMD studies [2, 3] that use the same PBE-D3 functional and temperatures, as well as with experimental data [5] collected at 295 K.

Benchmarks of the MLIP on bulk solution

We benchmark our fitted machine learning interatomic potential (MLIP) by comparing to previous *ab initio* molecular dynamics (AIMD) and experimental measurements on the structural and dynamical properties of pure water and aqueous KF solution.

Bulk water For pure bulk water, we compare the MLIP against previous AIMD simulations [1–3] and MLIP MD studies [3] based on the same DFT functional (PBE-D3) without nuclear quantum effect corrections. Consistent with the previous AIMD studies [1, 3], the system contains 64 water molecules at the density of 0.997 g/ml. The simulations were conducted using the ASE package [4] in the NVT ensemble using the Nosé-Hoover thermostat. Each trajectory has 500 ps with a 1 fs timestep after a 100 ps equilibration.

Fig. S1 compares the oxygen-oxygen RDFs $g_{OO}(r)$ and running coordination numbers $n_{OO}(r)$ for bulk water at 360 K, 370 K and 390 K. Experimental data (black dashed lines) at 295 K [5] are included for comparison. At both 360 K and 390 K, the RDFs from the

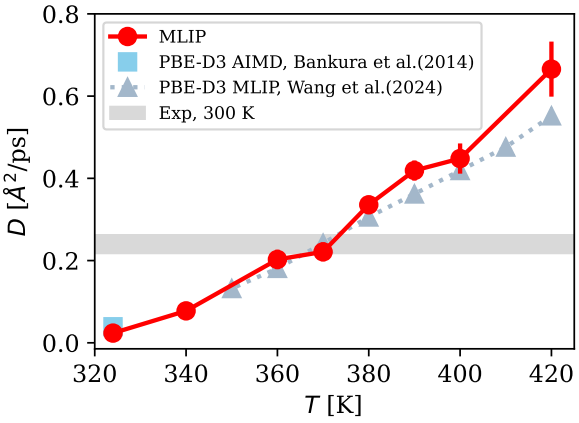

Figure S2. The temperature-dependent diffusion coefficient ($D(T)$). Red and blue lines represent NVT MD results from our MLIP and a previous NEP MLIP [3] at a fixed density of 0.997 g/ml, respectively. AIMD data [1] (blue square) and experimental values at room temperature [6–9] (gray band) are included for reference.

MLIP MD agree well with AIMD results. At 370 K, the RDF from the MLIP is quite close to the experiment at room temperature.

Fig. S2 shows the diffusion coefficients of water ($D(T)$) over the temperature range of 324 K-420 K, computed from the mean square displacement (MSD) via the Einstein relation without system size corrections. The MLIP results (red symbols) are in good agreement with previous studies based on the same DFT functional, including AIMD simulations [1, 10] (blue square) and a recent neuroevolution potential (NEP) study [3] (gray triangle). The MLIP D at the elevated temperature of 370 K matches the experimental diffusion coefficient of water at room temperature (gray band, 0.218-0.262 Å^2/ps) [6–9].

Bulk KF aqueous electrolyte To directly compare with a previous AIMD simulation [2] based on the PBE-D3 functional, we employed the same simulation box setup: 1 ion (either K^+ or F^-) and 63 water molecules in a periodic cubic cell of 12.42 Å, which corresponds to 0.9 M ion concentration. MLIP MD simulations were conducted at 390 K in the NVT ensemble using a Nosé–Hoover thermostat for 200 ps after 50 ps of equilibrium.

Fig. S3 shows the computed RDFs between the ions (K^+ and F^-) and the O atoms of water molecules, and the running coordination numbers $n_{\mathrm{IO}}(r)$ (i.e., the integrated RDF). It shows a good agreement between our MLIP and AIMD results for both $g_{\mathrm{FO}}(r)$ and $g_{\mathrm{KO}}(r)$. From the RDFs, the first solvation shell cutoffs are 3.65 Å for K^+ and 3.26 Å for F^-, con-

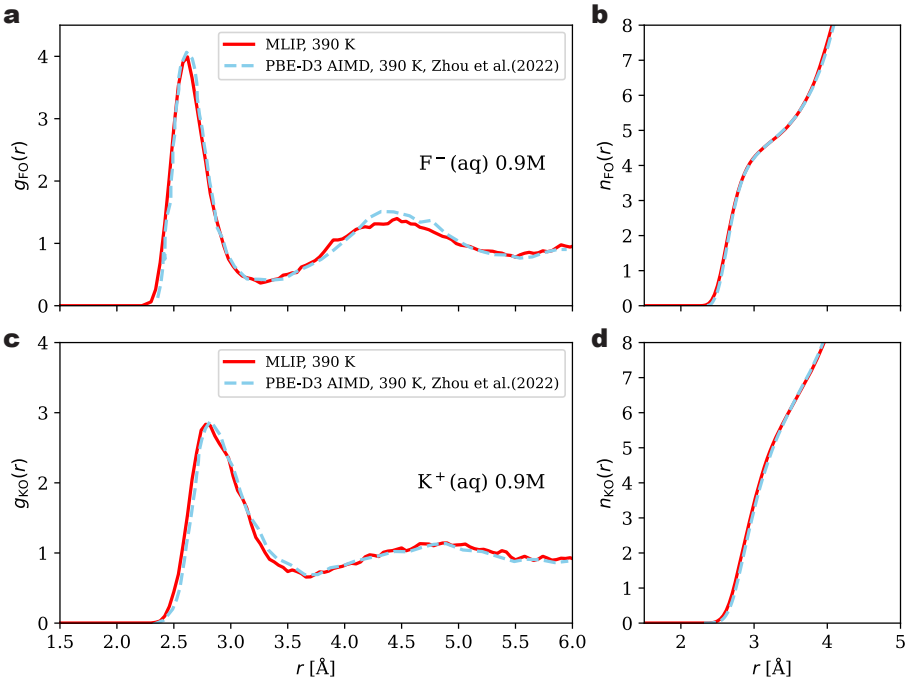

Figure S3. Ion-oxygen radial distribution functions ($g_{IO}(r)$) and running coordination numbers ($n_{IO}(r)$) of aqueous ion solutions at 390 K (red solid lines) with a concentration of 0.9 M. Previous AIMD results [2] at 390 K based on PBE-D3 (blue dashed lines) are included for comparison.

Table S1. Hydration shell properties for F^- and K^+ ions. The position (r_1) and intensity (g_1) of the first peak in RDFs, and the coordination numbers (n_{IO}) obtained by integrating from oxygen-ion RDFs to the first minimum (solvation shell cutoff) are tabulated for different research approaches. Previous AIMD results [2] and experimental data for 0.7-4 M KF solutions at 298 K [11, 12] are included for comparison.

Ion	Method	Condition	r_1 [Å]	g_1	n_{IO}
F^-	MLIP	370 K, 1.3 M KF	2.62	4.17	4.85
	MLIP	390 K, 0.9 M K^+(aq)	2.62	3.99	4.73
	AIMD	390 K, 0.9 M K^+(aq)	2.62	4.07	4.70
	Exp	298 K, 0.7-4 M KF	2.54-2.62 [11, 12]		4.5-6.9 [11, 12]
K^+	MLIP	370 K, 1.3 M KF	2.82	3.06	6.57
	MLIP	390 K, 0.9 M K^+(aq)	2.78	2.84	6.72
	AIMD	390 K, 0.9 M K^+(aq)	2.82	2.88	6.86
	Exp	298 K, 0.7-4 M KF	2.73-2.95 [11, 12]		5.3-6.4 [11, 12]

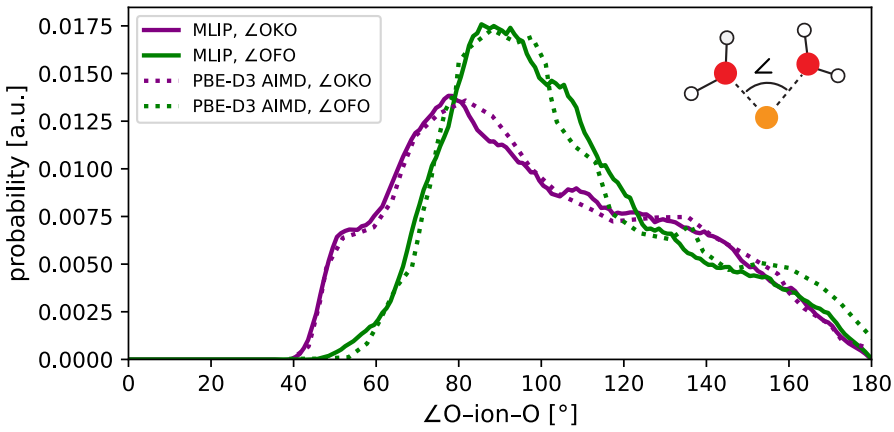

Figure S4. Distribution of the angles ∠O–ion–O for K^+ (purple) and F^- (green) at 390 K based on NVT simulations of a system of 1 ion (K^+ or F^-) and 63 water molecules. The angle ∠O–ion–O is illustrated in the insert. Previous AIMD results [2] at 390 K based on PBE-D3 (dashed lines) are included for comparison.

sistent with previous AIMD data [2] and experimental measurements by X-ray and neutron scattering or diffraction [11–14] (see Table S1). The structural information of hydration shells is also summarized in Table S1.

The ∠O–ion–O angle distributions within the first solvation shells of K^+ (purple line) and F^- (green line) are shown in Fig. S4. The ∠O–F–O distribution for the hydrated F^- ion is centered between 80° and 110°, which suggests a well-ordered shell consistent with tetrahedral ($n_{FO} = 4$) and pentahedral ($n_{FO} = 5$) coordination geometries. This structured arrangement inferred from ∠O–ion–O is consistent with the derived coordination number of $n_{FO} \approx 4.7$ computed from $g_{FO}(r)$, as shown in Fig. S3 and Table S1. In contrast, the ∠O–K–O angles exhibit a flattened distribution, which suggests a more flexible solvation shell of K^+ and its lower hydration free energy compared to F^-. These findings align with earlier theoretical studies on the thermodynamics of solvation of these two ions at 298 K [15, 16], which treat the ion and its first hydration shell with high-accuracy quantum mechanics and the remaining solvent with classical force fields.

We ran another set of MLIP MD simulations using a charge-neutral setup that is more akin to experiments: a cubic simulation box with a dimension of 18.50 Å containing 5 KF ion pairs and 208 water molecules, which corresponds to a KF 1.3 M solution. NVT simulations were performed at 370 K for 200 ps with a timestep of 1 fs after 50 ps of equilibrium. These

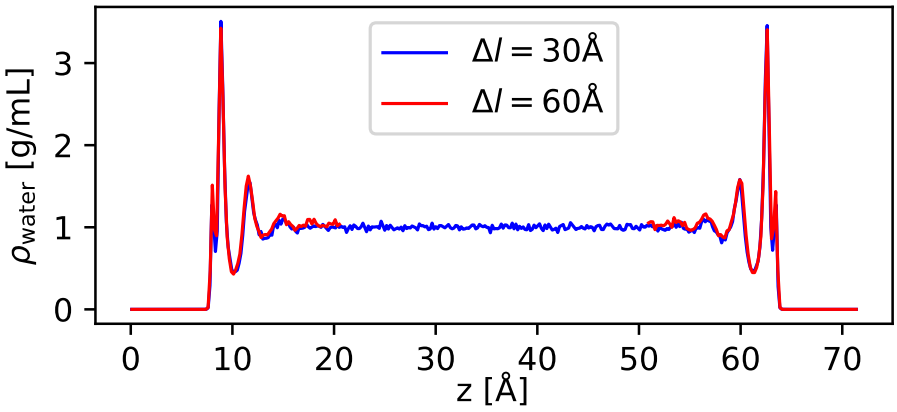

Figure S5. Comparison of water density distributions from simulations at 420 K of Pt(111)-water interfaces with different electrolyte thickness Δl.

computed hydration shell properties are listed in Table S1, which are similar to the ones using the isolated ions solvated in water.

Size convergence test

we have performed a convergence test using about double the system size: Fig. S5 compares the simulation using 1626 atoms (with electrolyte filled between the space of $\Delta l = 60$ Å between two Pt surfaces) at 420 K, and the simulation using 915 atoms (with electrolyte filled between the space of $\Delta l = 40$ Å between two Pt surfaces) produce consistent EDL structures.

Surface coverage of water

In Fig. S6 we show the surface coverage of water on the Pt(111) surfaces at different bias $\Delta\Phi$. The surface coverage percentage is the ratio between the number surface Pt atoms that have an oxygen atom with distance less than 2.7 Å and the total number of surface Pt atoms (36 atoms on the (6×6) 111 surface for each electrode). At the zero bias condition (PZC), the surface coverage is about 15%.

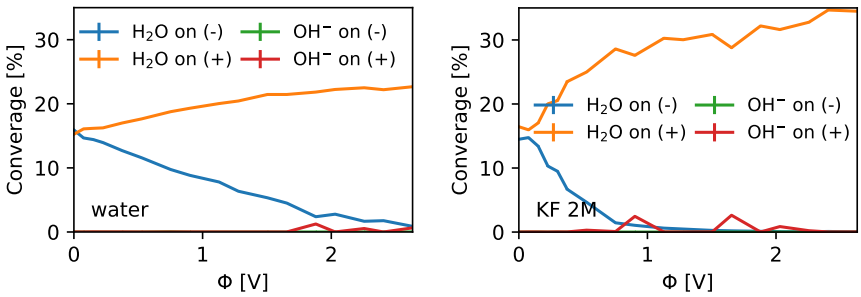

Figure S6. The surface coverage of water on the Pt(111) surfaces at different bias $\Delta\Phi$.

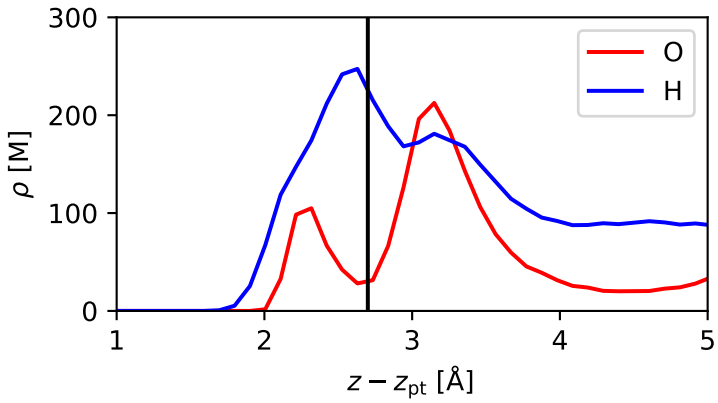

Figure S7. Oxygen and hydrogen molar density distributions for the Pt(111)-water system at 370 K and zero electric bias (PZC). The horizontal axis of the figure corresponds to the vertical distance to the top of the Pt surface.

Criteria for chemisorbed vs physisorbed water

We classify chemisorbed and physisorbed water molecules as: chemisorbed water molecules have oxygen positions within 2.7 Å of the Pt surface, and physisorbed water have oxygen positions within 2.7 Å to 4.5 Å to the surface. As shown in Fig. S7, the 2.7 Å correspond to the minimum in the oxygen density distribution, and the chemisorbed and physisorbed water distributions have well-separated peaks.

Snapshots of chemisorbed and physisorbed water molecules are provided in Fig. S8 and Fig. S9, respectively.

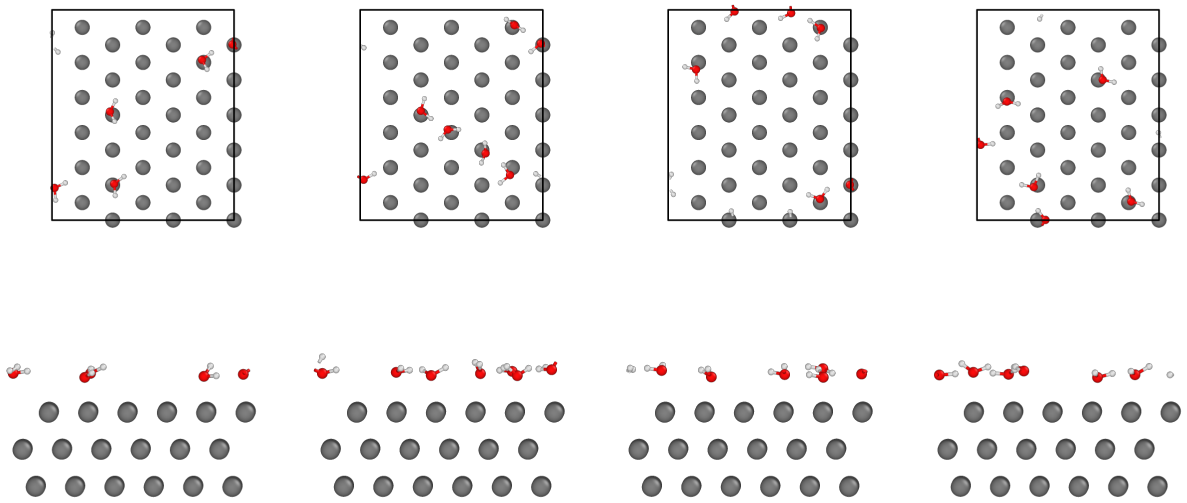

Figure S8. Snapshots for the chemisorbed water molecules on surface for the Pt(111)-water system at 370 K and zero electric bias (PZC).

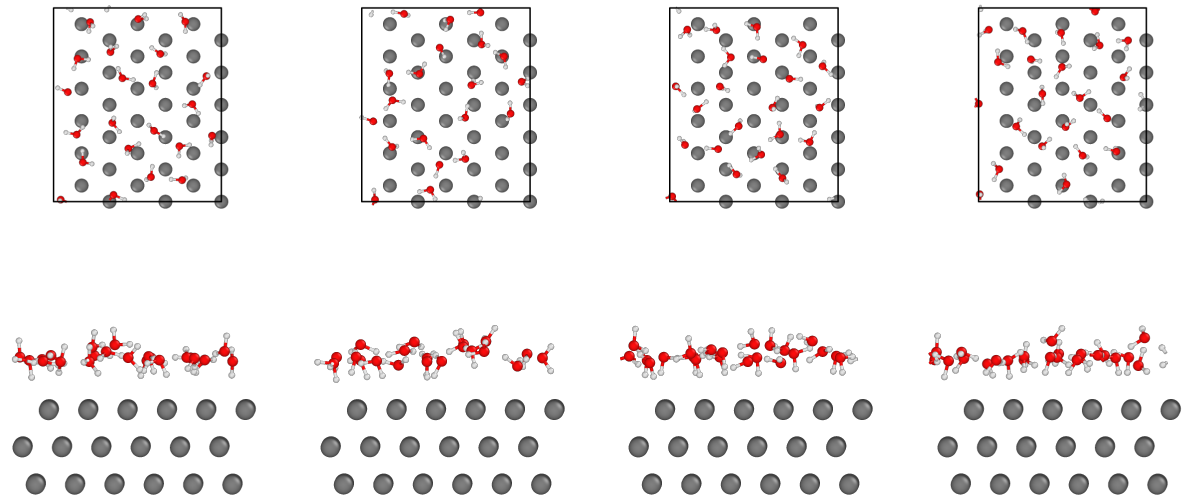

Figure S9. Snapshots for the physisorbed water molecules on surface for the Pt(111)-water system at 370 K and zero electric bias (PZC).

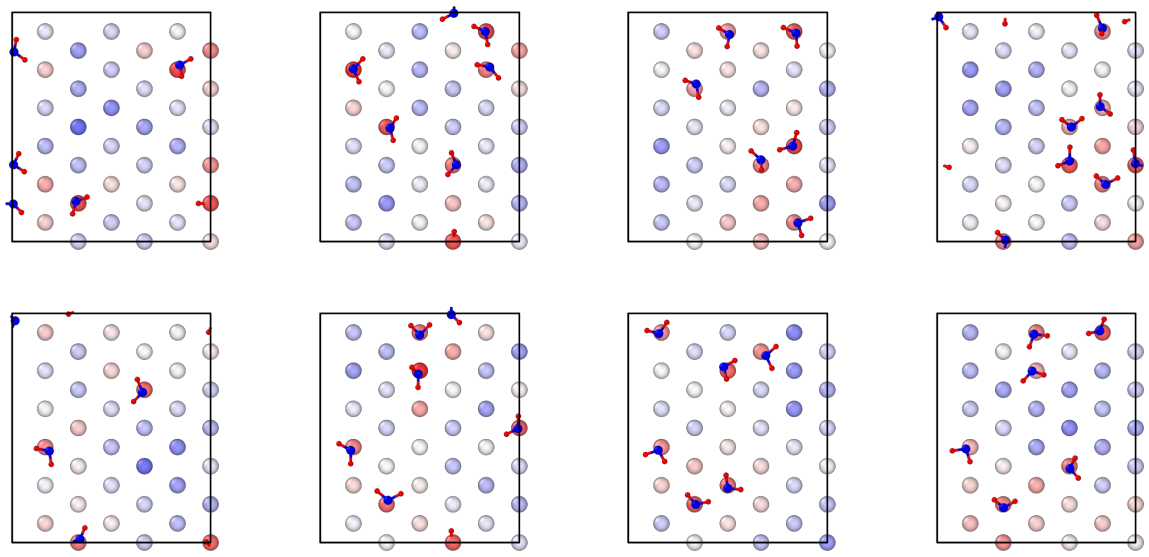

Figure S10. Snapshots for the surface charge distribution in the Pt(111)-water system at 370 K and zero electric bias (PZC). For clarity, only the chemisorbed water molecules are shown. Blue indicates negative charges, and red indicates positive charges.

Surface charge distribution

Fig. S10 shows the charge distribution on the Pt surface for the Pt(111)-water interface. For clarity, only the surface layer of Pt atoms and the chemisorbed water molecules are shown. The Pt atoms that are vertically under the oxygen atoms of the chemisorbed water are positively charged (colored in red), while the surrounding Pt atoms are negatively charged (in blue). This picture seems quite intuitive considering the Siepmann-Sprik model used. It is also consistent with the diagonal transfer of charges from water to Pt atoms observed in a DFT study from Surendralal et al. [17]: in contrast with the conventional view that the electron transfer is vertical (from the on-top bonded water molecule to the Pt atom below), both the water molecule and the on-top Pt atom act as electron donors, while the nearby Pt atoms become negatively charged.

Fig. S11 shows the charge distribution for the Pt(111)-KF 2M interface. F^- within 4.5 Å and chemisorbed water molecules are shown. The surface charge distributions are similar to the pure water case, except that F^- seems to induce a smaller amount of positive charges on the metal atom beneath.

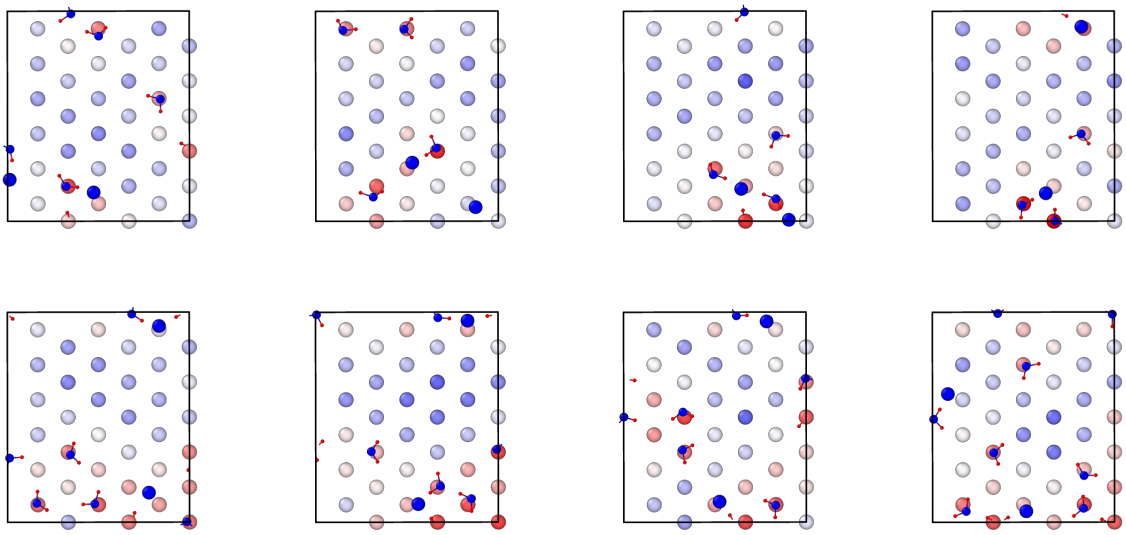

Figure S11. Snapshots for the surface charge distribution in the Pt(111)-KF 2M system at 370 K and zero electric bias (PZC). For clarity, only the chemisorbed water molecules and F^- (medium sized blue spheres) within 4.5 Å of the Pt surface are shown. Blue indicates negative charges, and red indicates positive charges.

Diffusion coefficient of water in Pt(111)-water and Pt(111)-KF 2M interfaces

As depicted in Fig. 1a of the main text, the interface system is divided into five distinct zones along the z-axis: a chemisorbed layer ($\leq$2.7 Å from the surface) and a physisorbed layer (2.7–4.5 Å from the surface) close to the cathode ($-$), the two layers close to the anode ($+$), and the bulk region with distance $\geq$10 Å away from the Pt surface. Fig. S12 shows the in-plane (D_{xy}) and out-of-plane (D_z) diffusion coefficients of undissociated water molecules across these five regions for Pt(111)-water, Pt(111)-0.4 M KF, and Pt(111)-2 M KF systems, computed using the MSD of water molecules that are initially in the corresponding region.

In all the systems, interfacial water molecules show reduced diffusivity compared to the bulk ones at zero bias conditions ($\Delta\Phi = 0$ V). However, at finite $\Delta\Phi$, the in-plane mobilities of the interfacial water at the cathode are enhanced and can exceed the bulk values.

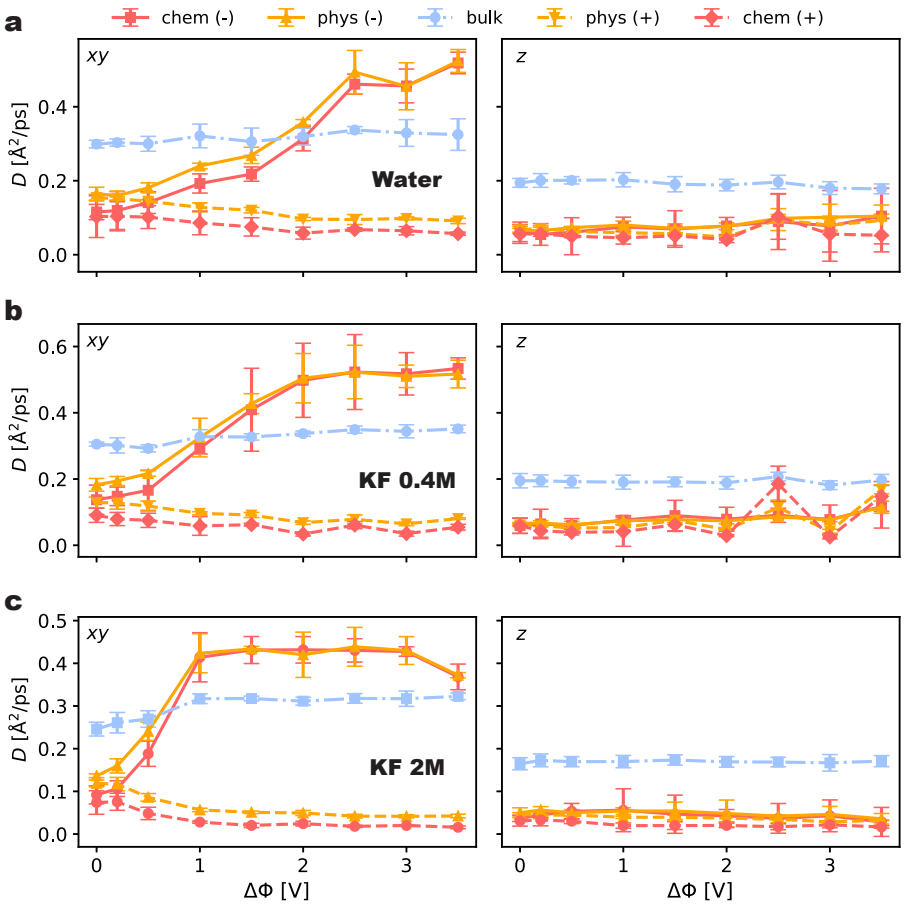

Figure S12. In-plane (D_{xy}) and out-of-plane (D_z) diffusion coefficients of water in five distinct regions for three systems: (a) the Pt(111)-water interface, (b) the Pt(111)-0.4 M KF interface, and (c) the Pt(111)-2 M KF interface. Results are shown for regions near the cathode (−, solid lines) and the anode (+, dashed lines). The chemisorbed (chem, red) and physisorbed (phys, orange) layers are defined by their distance to the surface of the cathode and anode, ≤2.7 Å and 2.7-4.5 Å, respectively. The bulk region (blue) is at a distance of ≥10 Å away from the Pt surface.

Water dissociation and proton transfer reactions

In Fig. 2 of the main text, we provide two representative trajectories of reactions, as well as the aggregated proton transfer analysis across different bias potentials $\Delta\Phi$. Here we show the individual analysis for each simulation run where water dissociation occurred.

Fig. S13 shows the water dissociation reaction for the Pt(111)-water, and Fig. S14 shows the reaction for the Pt(111)-aqueous KF 2 M system at 370 K under different bias potentials $\Delta\Phi$. We visualize all these water dissociation reactions using two consecutive snapshots: The

first snapshot shows the last configuration before water dissociation has happened with the simulation time t indicated, and the second snapshot shows the dissociated configuration at time $t + 1$ ps.

The individual proton transfer statistics for H_3O^+ and Pt-OH in Pt(111)-water (Fig. S15) and Pt(111)-aqueous KF 2 M (Fig. S16) systems are analyzed using the same methodology described in the main text. From each trajectory, we used a maximum of 500 ps after dissociation for the analysis. Such individual analyses confirm that a Poisson model (orange lines) parameterized by τ effectively describes proton hopping dynamics for both hydronium and hydroxide. Figs. S15 and S16 also suggest that the mean hopping time τ does not have a clear dependence on the applied potential $\Delta\Phi$. Consequently, the values for τ reported in the main text were aggregated from these individual analyses.

Diffusion coefficients of H_3O^+ and Pt-OH

To further confirm that added ions reduce the proton transfer rate of H_3O^+ and Pt-OH in the Pt(111)-aqueous interface systems, we compute the diffusion coefficients based on the mean square displacements in the x-y plane. As with the hopping statistics, no systematic dependence on $\Delta\Phi$ was observed, so values were averaged across all finite-field simulations. The in-plane diffusion coefficient was computed using the MSD along x and y directions according to the Einstein relation:

$$D = \frac{\langle \Delta r^2(t) \rangle}{4t}, \tag{1}$$

where $\langle \Delta r^2(t) \rangle$ is the ensemble-averaged MSD in two dimensions and t is the elapsed time. The total time lag in computing MSD was 10 ps, and D was obtained from the slope between 2-10 ps. For the Pt(111)-water interface, the diffusion coefficients are $D = 2.95(8)$ Å^2/ps for H_3O^+ and $D = 0.56(2)$ Å^2/ps for Pt-OH, consistent with the faster mobility of the excess proton. Upon addition of 2 M KF, both species exhibit reduced diffusivity: $D = 1.43(5)$ Å^2/ps for H_3O^+ and $D = 0.47(2)$ Å^2/ps for Pt-OH. These H_3O^+ diffusion coefficients are quite consistent with what a memory-less random jump model in 3D combined with the computed proton hopping τ: 1.6 Å^2/ps for water and 1.0 Å^2/ps for KF 2 M, when taking the oxygen-oxygen nearest neighbor distance to be 2.85 Å. On the contrary, the 2D random model predicts the Pt-OH diffusion coefficients 1.1 Å^2/ps for water and 0.9 Å^2/ps for KF

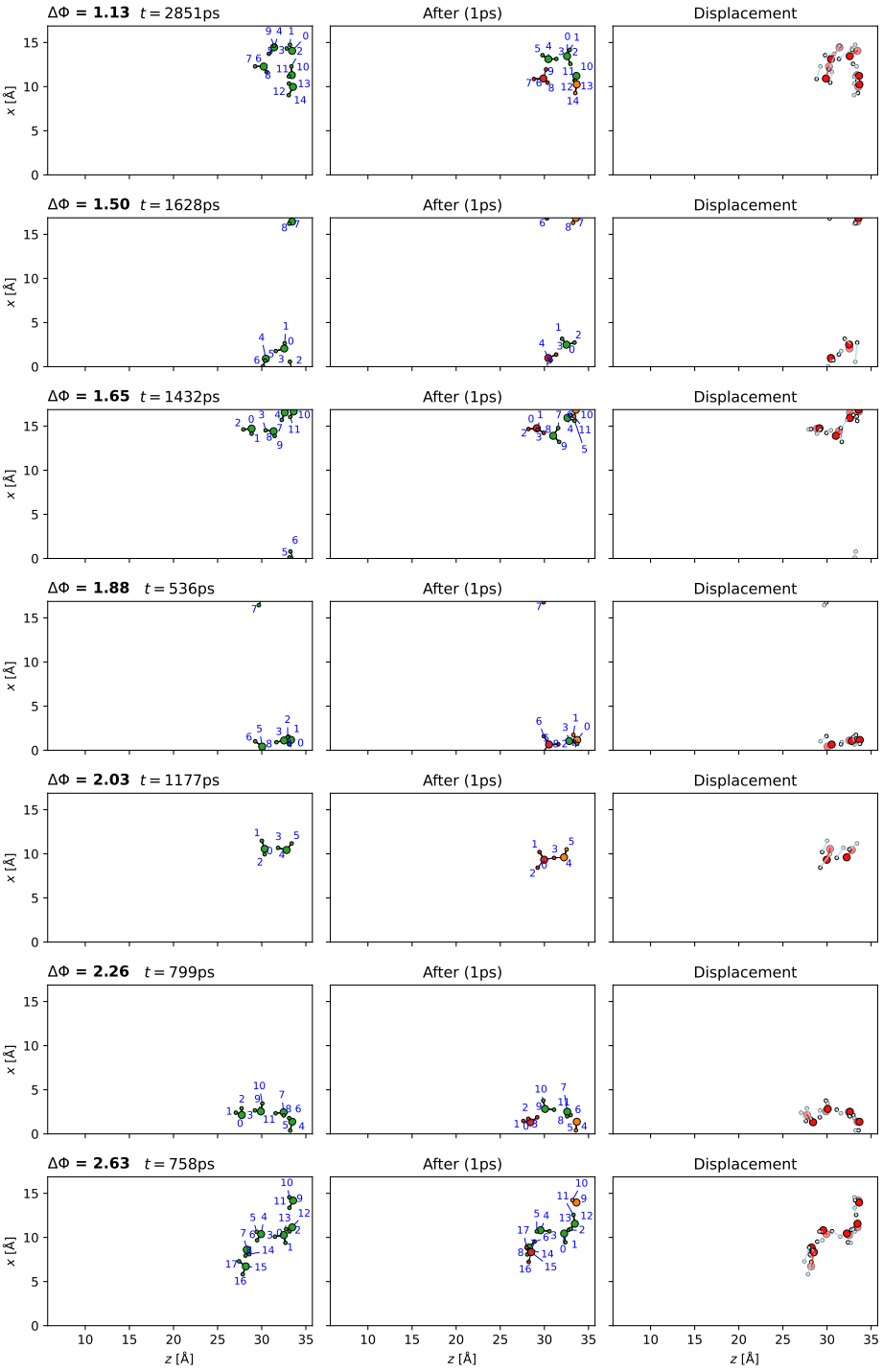

Figure S13. Configurations before and after water dissociation, in the Pt(111)-water system at 370 K and under different bias potentials $\Delta\Phi$. The first column shows the snapshot before dissociation. The onset time for water dissociation is indicated. The second column shows the snapshot 1 ps after the first snapshot. Water molecules are marked in green, H_3O^+ ions are marked in red, OH ions are marked in orange. Atoms from species participating in the reactions are indexed. The third column demonstrates the displacement of the relevant atoms during the 1 ps interval. Oxygen atoms are in red, and hydrogen atoms are in white.

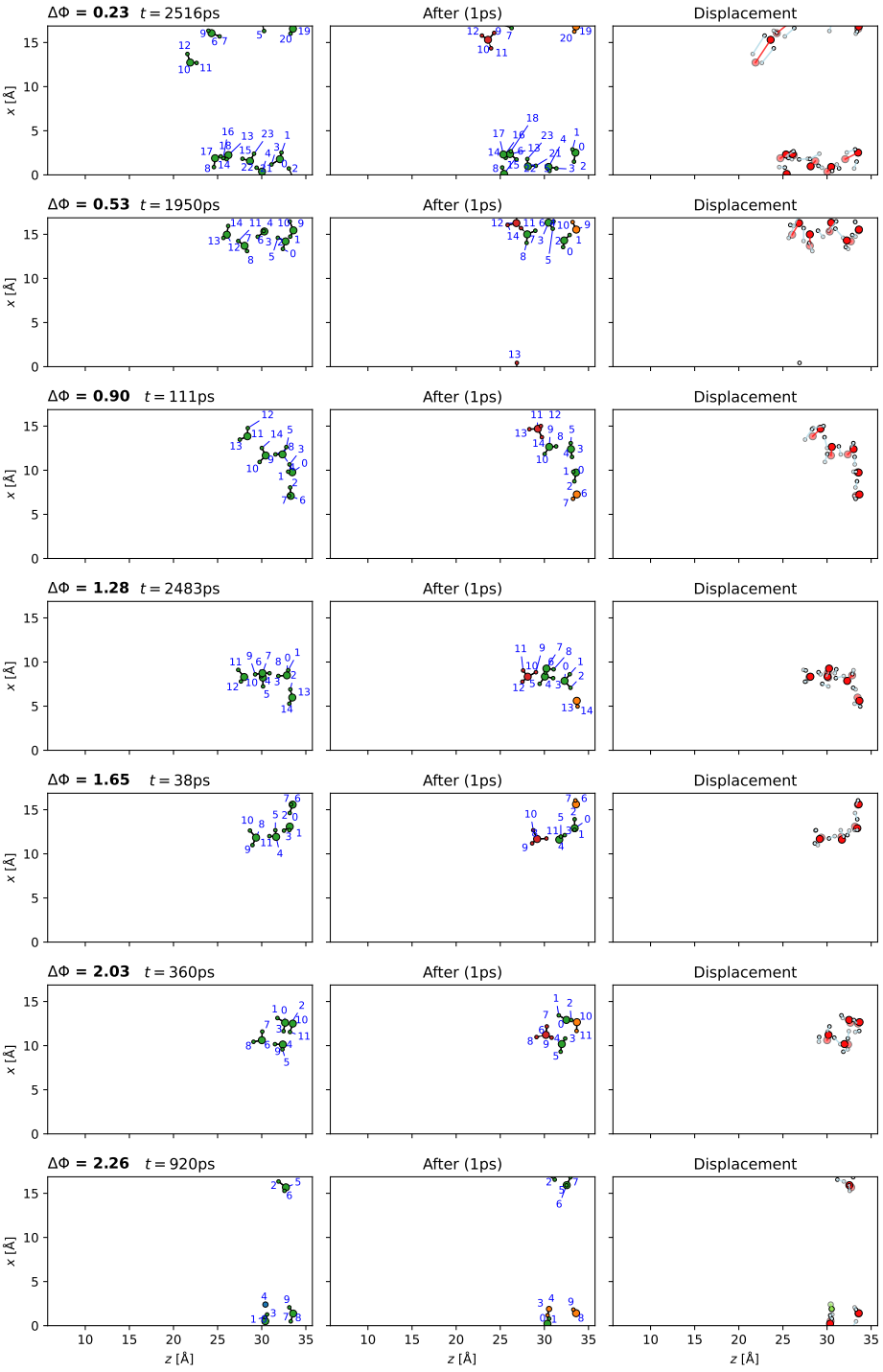

Figure S14. Configurations before and after water dissociation, in the Pt(111)-aqueous KF 2 M system at 370 K and under different bias potentials $\Delta\Phi$. The first column shows the snapshot before dissociation. The onset time for water dissociation is indicated. The second column shows the snapshot 1 ps after the first snapshot. Water molecules are marked in green, H_3O^+ ions are marked in red, OH ions are marked in orange. HF is marked in orange at the bottom middle panel. Atoms from species participating in the reactions are indexed. The third column demonstrates the displacement of the relevant atoms during the 1 ps interval. Oxygen atoms are in red, hydrogen atoms are in white, and floride atoms are in green.

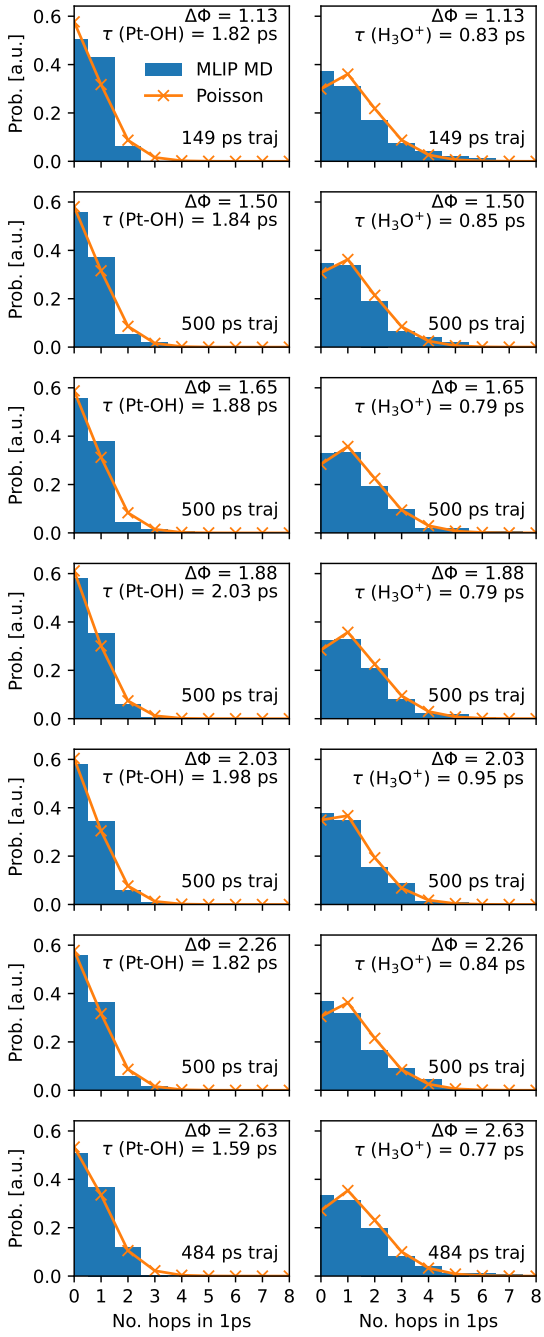

Figure S15. Distribution of proton-hopping events per picosecond for hydroxide (left column) and hydronium (right column) in the Pt(111)-water system at 370 K under a set of bias potentials $\Delta\Phi$. Simulation data (blue bars) were obtained from MD trajectories after water dissociation occurred, compared with Poisson distributions (orange lines) parameterized by the mean hopping time τ.

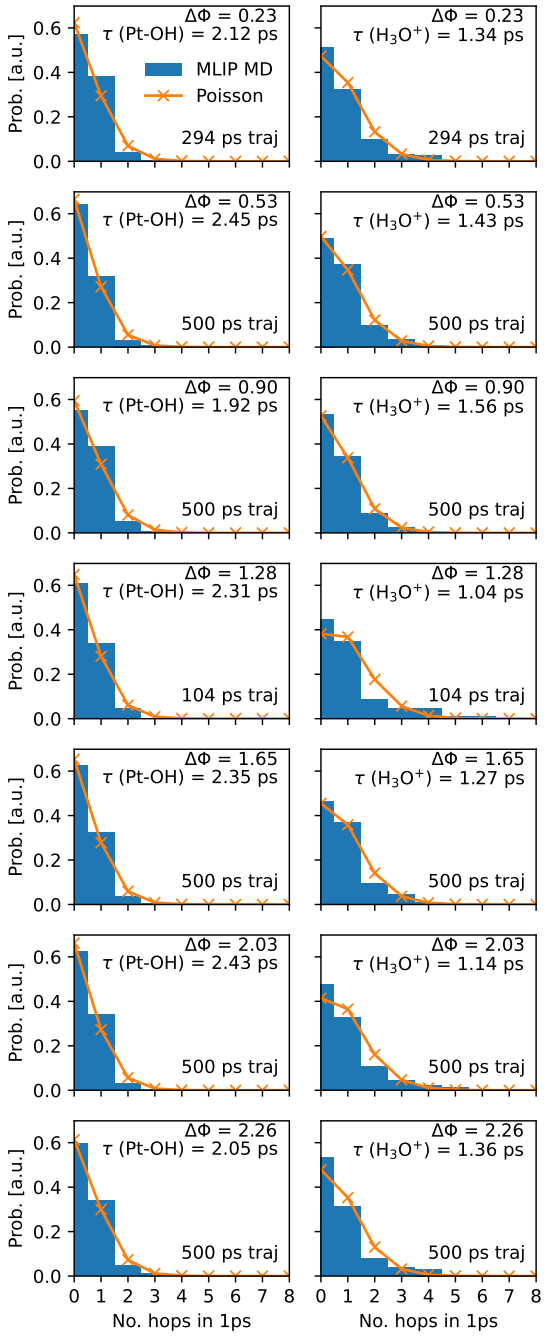

Figure S16. Distribution of proton-hopping events per picosecond for hydroxide (left column) and hydronium (right column) in the Pt(111)-aqueous KF 2 M system at 370 K under a set of bias potentials $\Delta\Phi$. Simulation data (blue bars) were obtained from MD trajectories after water dissociation occurred, compared with Poisson distributions (orange lines) parameterized by the mean hopping time τ.

2 M, which are faster than the computed D values. This can be explained by the back-and-forth jumping observed in the inverse Grotthuss step.

---

[1] A. Bankura, A. Karmakar, V. Carnevale, A. Chandra, and M. L. Klein, "Structure, dynamics, and spectral diffusion of water from first-principles molecular dynamics," The Journal of Physical Chemistry C **118**, 29401 (2014).

[2] K. Zhou, C. Qian, and Y. Liu, "Quantifying the structure of water and hydrated monovalent ions by density functional theory-based molecular dynamics," The Journal of Physical Chemistry B **126**, 10471 (2022).

[3] C. Wang, W. Tian, and K. Zhou, "*Ab initio* simulation of liquid water without artificial high temperature," Journal of Chemical Theory and Computation **20**, 8202 (2024).

[4] A. H. Larsen, J. J. Mortensen, J. Blomqvist, I. E. Castelli, R. Christensen, M. Dułak, J. Friis, M. N. Groves, B. Hammer, C. Hargus, *et al.*, "The atomic simulation environment—a Python library for working with atoms," Journal of Physics: Condensed Matter **29**, 273002 (2017).

[5] L. B. Skinner, C. Benmore, J. C. Neuefeind, and J. B. Parise, "The structure of water around the compressibility minimum," The Journal of Chemical Physics **141**, 214507 (2014).

[6] J. H. Wang, "Self-diffusion coefficients of water," The Journal of Physical Chemistry **69**, 4412 (1965).

[7] L. Korson, W. Drost-Hansen, and F. J. Millero, "Viscosity of water at various temperatures," The Journal of Physical Chemistry **73**, 34 (1969).

[8] M. Holz, S. R. Heil, and A. Sacco, "Temperature-dependent self-diffusion coefficients of water and six selected molecular liquids for calibration in accurate 1H NMR PFG measurements," Physical Chemistry Chemical Physics **2**, 4740 (2000).

[9] P. S. Tofts, D. Lloyd, C. Clark, G. Barker, G. Parker, P. McConville, C. Baldock, and J. Pope, "Test liquids for quantitative MRI measurements of self-diffusion coefficient in vivo," Magnetic Resonance in Medicine **43**, 368 (2000).

[10] M. J. Gillan, D. Alfe, and A. Michaelides, "Perspective: How good is DFT for water?" The Journal of Chemical Physics **144** (2016).

[11] H. Ohtaki and T. Radnai, "Structure and dynamics of hydrated ions," Chemical Reviews **93**, 1157 (1993).

[12] A. K. Soper and K. Weckström, "Ion solvation and water structure in potassium halide aqueous solutions," Biophysical Chemistry **124**, 180 (2006).

[13] V.-A. Glezakou, Y. Chen, J. L. Fulton, G. K. Schenter, and L. X. Dang, "Electronic structure, statistical mechanical simulations, and EXAFS spectroscopy of aqueous potassium," Theoretical Chemistry Accounts **115**, 86 (2006).

[14] J. Mahler and I. Persson, "A study of the hydration of the alkali metal ions in aqueous solution," Inorganic Chemistry **51**, 425 (2012).

[15] T. S. Hofer and P. H. Hünenberger, "Absolute proton hydration free energy, surface potential of water, and redox potential of the hydrogen electrode from first principles: QM/MM MD free-energy simulations of sodium and potassium hydration," The Journal of Chemical Physics **148** (2018).

[16] T. S. Hofer, "Solvation structure and ion–solvent hydrogen bonding of hydrated fluoride, chloride and bromide—a comparative QM/MM MD simulation study," Liquids **2**, 445 (2022).

[17] S. Surendralal, M. Todorova, and J. Neugebauer, "Impact of water coadsorption on the electrode potential of h-pt(1 1 1)-liquid water interfaces," Physical Review Letters **126** (2021), 10.1103/physrevlett.126.166802.